BIOCHEMISTRY
including biophysical chemistry & molecular biology
Article

Biochemistry **2009,** *48,* 6921–6931 6921
DOI: 10.1021/bi900897h

Catalytic Mechanism of SHCHC Synthase in the Menaquinone Biosynthesis of *Escherichia coli*: Identification and Mutational Analysis of the Active Site Residues†

Ming Jiang,‡ Xiaolei Chen,‡ Xian-Hui Wu,§ Minjiao Chen,‡ Yun-Dong Wu,§ and Zhihong Guo*,‡

‡*Department of Chemistry, Center for Cancer Research, The Hong Kong University of Science and Technology, Clear Water Bay, Kowloon, Hong Kong SAR, China, and* §*Laboratory of Chemical Genomics, Shenzhen Graduate School of Peking University, Shenzhen, China*

Received September 3, 2008; Revised Manuscript Received June 22, 2009

ABSTRACT: (1*R*,6*R*)-2-Succinyl-6-hydroxy-2,4-cyclohexadiene-1-carboxylate (SHCHC) synthase (MenH) is an α/β fold enzyme containing a catalytically essential serine−histidine−aspartate triad typical of serine proteases but catalyzes a pyruvate elimination reaction initiated by α-proton abstraction in the menaquinone biosynthetic pathway of *Escherichia coli*. In this study, we identify the active site residues in the synthase through sequence analysis and structural modeling and study their mechanistic roles in MenH catalysis. Steady-state kinetic characterization of site-directed mutants of the active site residues shows that three conserved arginine residues (Arg-90, Arg-124, and Arg-168) likely form ionic salt bridges with three carboxylate groups of the substrate in the Michaelis complex and that the side-chain polar groups of the conserved tyrosine (Tyr-85) and tryptophan (Trp-147) residues likely donate hydrogen bonds to form an "oxyanion hole". In addition, the pH dependence of the MenH kinetic properties reveals a catalytic base with a pK_a highly dependent on the hydroxyl group of the triad serine residue in the enzymatic reaction. Moreover, proton inventory experiments demonstrate that the SHCHC synthase adopts one-proton catalysis like many serine proteases. These results allow the proposal of a mechanism in which the histidine residue of the MenH triad serves as a general base catalyst to deprotonate the triad seryl hydroxyl group in the α-proton abstraction from the substrate. As such, the MenH triad performs a simple and fundamental proton transfer reaction occurring repeatedly in the reactions catalyzed by serine proteases and α/β fold hydrolases, suggesting a common evolutionary origin for all serine−histidine−aspartate triads serving different catalytic functions.

(1*R*,6*R*)-2-Succinyl-6-hydroxy-2,4-cyclohexadiene-1-carboxylate (SHCHC)[1] synthase, or MenH, is involved in the biosynthesis of menaquinone, a lipid-soluble metabolite functioning as an electron carrier in the respiratory chain of many microorganisms including facultative *Escherichia coli* (*1*, *2*). It has been found to catalyze a pyruvate elimination reaction, which is initiated by abstraction of the cyclohexene ring α-proton of the succinyl group of its substrate SEPHCHC (Figure 1A) (*3*, *4*). This catalytic activity shares the same partial reaction with many enzymes catalyzing proton abstraction reactions, which include those in the enolase superfamily (*5*, *6*). However, MenH adopts an α/β hydrolase fold and relies its activity on a Ser-His-Asp triad typical of serine proteases and a large number of enzymes in the α/β hydrolase superfamily (*4*). Concomitantly, the synthase exhibits a significant level of sequence homology to the C−C bond hydrolase MhpC. This close resemblance of the synthase to α/β hydrolases may have led to the previous proposal that MenH is a thioesterase responsible for the hydrolysis of 1,4-dihydroxynaphthoyl-CoA (DHNA-CoA) (*2*, *7*), another necessary step in the menaquinone biosynthetic pathway.

Besides its biological function, the catalytic mechanism of the SHCHC synthase is also unpredictable from its amino acid sequence, its crystallographic structure, or even its catalytic triad. It is well-known that most serine proteases (*8*, *9*) and α/β fold hydrolases (*10*, *11*) adopt a catalytic mechanism in which an acyl-enzyme intermediate is involved (Figure 1B). The triad serine residue is deprotonated to generate an oxyanion for nucleophilic addition to the scissile bond of the substrate in the formation of the acyl-enzyme intermediate, while the histidine residue serves alternately between a general base and a general acid as the enzymatic reaction progresses through the catalytic steps. For the C−C bond α/β fold hydrolase MhpC to which MenH is most similar in both amino acid sequence and three-dimensional structure, it first catalyzes a keto−enol tautomerization (*12*) and then deprotonates an active site water to attack the substrate carbonyl to effect C−C bond cleavage (*13*, *14*). In this enzymic

†This work was financially supported by HKUST and RGC of the Hong Kong SAR government.

*Corresponding author. Tel: 852-2358-7352. Fax: 852-2358-1594. E-mail: chguo@ust.hk.

[1]Abbreviations: SEPHCHC, (1*R*,2*S*,5*S*,6*S*)-2-succinyl-5-enolpyruvyl-6-hydroxy-3-cyclohexene-1-carboxylate; SHCHC, (1*R*,6*R*)-2-succinyl-6-hydroxy-2,4-cyclohexadiene-1-carboxylate; IPTG, isopropyl β-D-thiogalactopyranoside; MhpC, the C−C bond hydrolase (2-hydroxy-6-ketonona-1,9-dioic acid 5,6-hydrolase) in the phenylpropionic acid catabolic pathway; BSA, bovine serum albumin; KSI, Δ^5-3-ketosteroid isomerase; DTNB, dithiobis(nitrobenzoic acid).

Published on Web 06/22/2009

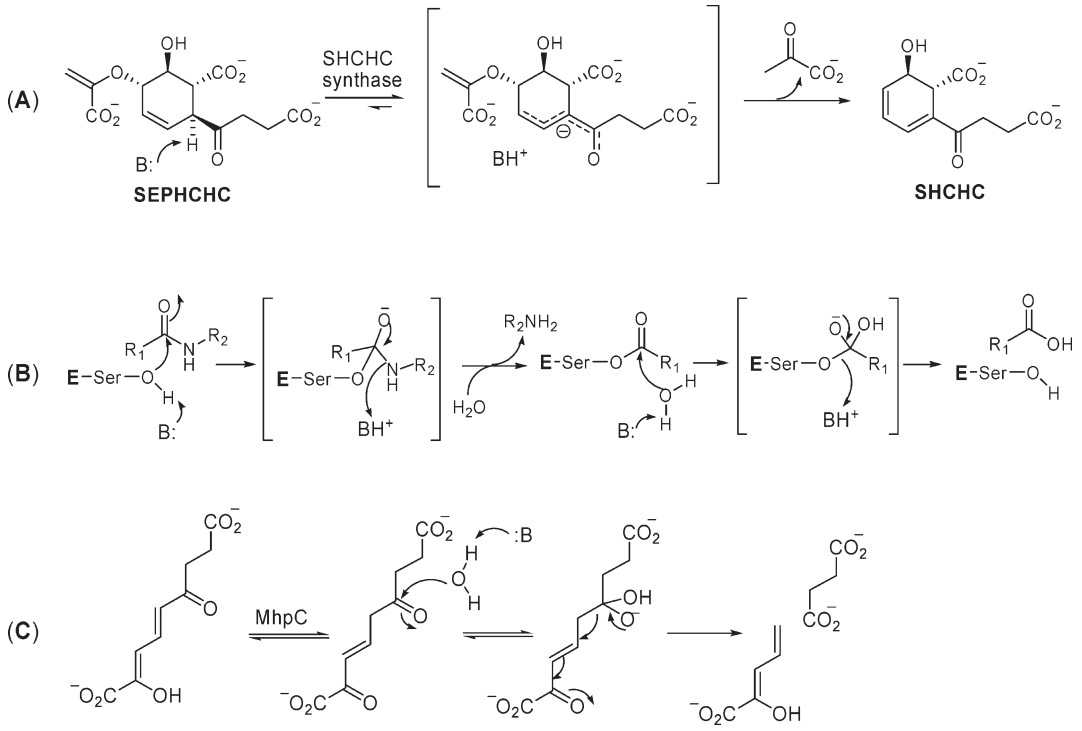

FIGURE 1: Reactions catalyzed by enzymes containing a Ser-His-Asp catalytic triad. (A) The MenH-catalyzed SHCHC synthesis. (B) The general reaction of peptide hydrolysis catalyzed by serine proteases. (C) The hydrolytic cleavage of a carbon−carbon bond adjacent to a carbonyl group by the C−C bond α/β hydrolase MhpC.

reaction (Figure 1C), the triad serine plays no nucleophilic role, and no acyl-enzyme intermediate is formed (*15*). Nevertheless, the triad histidine still serves multiple roles as both a general base and a general acid as in the catalysis of most serine proteases and other α/β fold hydrolases. In contrast, only a simple α-proton abstraction is needed in the reaction catalyzed by the SHCHC synthase to initiate the thermodynamically favorable pyruvate elimination (*4*).

Mutational studies have shown that the serine residue of the MenH triad seems to play a nonessential role in the SHCHC synthase activity (*4*), similar to the nonnucleophilic role for the serine residue in the MhpC triad (*13*). This similarity suggests that the general base catalysis required in the MenH-catalyzed reaction could be fulfilled by the catalytic triad in the same way as the α-proton abstraction by the histidine residue of the MhpC triad in the reverse enolization of the first half-reaction (*14*, *16*). However, it remains unknown whether the MenH triad undergoes splitting into an Asp-His dyad and an orphan serine like the MhpC triad (*14*). In addition, it is not known what role the serine residue of the triad plays in the catalysis. To answer these mechanistic problems, we attempt in this study to identify active site residues other than the catalytic triad in the synthase by a combination of amino acid sequence analysis, site-directed mutagenesis, and computer-based structural modeling. We also investigate the pH dependence of the enzyme kinetics and proton inventory of the enzymatic reaction in order to shed light on the roles of the catalytic triad in MenH and the intriguing catalytic mechanism adopted by the SHCHC synthase.

MATERIALS AND METHODS

General Information. Chemical reagents, including chorismate, α-ketoglutarate, thiamin diphosphate (ThDP), isopropyl β-D-thiogalactopyranoside (IPTG), buffers, and salts were purchased from Sigma. Other chemicals and biochemicals in reagent kits were purchased from vendors as specified below. UV−vis absorbance was measured using a Perkin-Elmer Lambda 900 UV/vis/NIR spectrometer. Polymerase chain reaction (PCR) amplifications were performed with a PTC-200 Peltier thermal cycler from MJ Research. Protein chromatography was performed on a Bio-Rad BioLogic HR workstation in a refrigerated chamber.

Site-Directed Mutagenesis. The QuikChange site-directed mutagenesis kit (Stratagene) was used to introduce the point mutations into MenH. The plasmid obtained previously for MenH expression (*4*) was used as the template in the mutagenic reactions. Oligodeoxynucleotides carrying the mutated sequences are listed in Table 1.

Expression and Purification of MenH and Its Mutants. Expression and purification of MenH and its mutants followed the procedures described previously (*4*). The recombinant proteins were expressed in BL21(DE3) in Luria broth containing 0.1 mM IPTG at 18 °C for 16 h and purified to greater than 95% in purity by a combination of metal chelating chromatography and gel filtration. The purified proteins were quantified by a Coomassie Blue protein assay kit (Pierce) and stored in 50 mM Tris-HCl buffer (pH 7.8) containing 10% glycerol and 50 mM NaCl at −20 °C until use.

Substrate Preparation and Enzyme Activity Assays. The SHCHC synthase substrate, SEPHCHC, was prepared from chorismate and 2-ketoglutarate using the isochorismate synthase EntC and SEPHCHC synthase MenD as previously described (*17*). The SHCHC synthase activity of wild-type MenH and its various mutants was measured by the increase of absorbance at 290 nm due to the formation of SHCHC, following the reported procedure (*4*). All kinetic assays were carried out in 50 mM phosphate buffer (pH 7.0) containing 0.1% BSA at 25 ± 0.5 °C. Control assays without enzyme were performed in the same buffer, and the absorbance changes caused by the spontaneous conversion of

Table 1: Oligodeoxynucleotide Primers Used in Site-Directed Mutagenesis of MenH

mutants	forward primer	reverse primer
Y85F	CTTCTGGCTGGTGGGGTTCTCACTTGGTGGACGGGTG	CACCCGTCCACCAAGTGAGAACCCCACCAGCCAGAAG
S86A	CTGGCTGGTGGGGTACGCACTTGGTGGACGGGTG	CACCCGTCCACCAAGTGCGTACCCCACCAGCCAG
R90A	GGTACTCGCTTGGTGGAGCGGTGGCGATGATGGC	GCCATCATCGCCACCGCTCCACCAAGCGAGTACC
R124A	GAACAACGTGCGGAAGCTCAGCGTTCCGATCGCC	GGCGATCGGAACGCTGAGCTTCCGCACGTTGTTC
D210A	GTGGTGAACGTGCTAGCAAATTCCGCGCCCTG	CAGGGCGCGGAATTTGCTAGCACGTTCACCAC
K212A	GGTGAACGTGACAGCGCATTCCGCGCCCTGGC	GCCAGGGCGCGGAATGCGCTGTCACGTTCACC
H232A	CATTCCTCGCGCCGGCGCTAACGCGCATCGGG	CCCGATGCGCGTTAGCGCCGGCGCGAGGAATG
H232K	CATTCCTCGCGCCGGAAAAAACGCGCATCGGG	CCCGATGCGCGTTTTTTCCGGCGCGAGGAATG
W147A	GCGGTATTTGCCGACGCGTATCAACAGCCTG	CAGGCTGTTGATACGCGTCGGCAAATACCGC
D128A	GGAACGTCAGCGTTCCGCCCGCCAATGGGTGCAGC	GCTGCACCCATTGGCGGGCGGAACGCTGACGTTCC
W147F	GCGGTATTTGCCGACTTCTATCAACAGCCTG	CAGGCTGTTGATAGAAGTCGGCAAATACCGC
R168A	GAGCTGGTGGCGCTGGCCAGCAACAATAATGGC	GCCATTATTGTTGCTGGCCAGCGCCACCAGCTC

SEPHCHC to SHCHC were subtracted from the value for the enzymic reactions.

In determination of the pH−rate profiles for the wild-type MenH and its S86A mutant, a series of buffers containing 50 mM sodium phosphate and 0.1% BSA were prepared with an increasing pH (4.5−10) at an interval of 0.25 pH unit. The kinetic parameters k_{cat} and K_M were determined at 25 ± 0.5 °C by measuring the initial velocity as described above. The rate of the spontaneous conversion of SEPHCHC to SHCHC was determined in the same buffer with a varied pH for correction of the value for the enzymic reaction. In proton inventory experiments, the MenH-catalyzed reactions were carried out in 50 mM phosphate buffer containing D_2O with an isotope fraction of $n = 0-1$ at pL = 8.75−8.85. The pL value was calculated using the formula pL = (pH meter reading) + $(0.076n^2 + 0.3314n)$ (*18*). Each velocity data point was the average of three independent measurements at one D_2O mole fraction. In these kinetic isotope effect studies, the concentration of SEPHCHC was 50 and 200 μM for wild-type MenH and its S86A mutant, respectively.

The MenH thioesterase activity was assayed using a method modified from a previously reported couple assay (*4*, *19*). The newly released free thiol was monitored in real time at 412 nm in the presence of excess Ellman's reagent (dithiobis(nitrobenzoic acid) (DTNB)). The assay was carried out in phosphate buffer (pH 7.5) containing 100 μM thioester substrates and 0.3 μg/mL MenH.

Sequence Analysis and Structural Modeling. Multiple sequence alignment was performed using Clustal X version 2.0 (*20*). The structural modeling of *E. coli* MenH from the crystal structure of MenH from *Vibrio cholerae* (PDB code 1R3D, 1.9 Å) was done with SWISS-MODEL (*21*), while the MenH−SEPHCHC complex was modeled with AutoDock 3.0.5 (*22*). The energy-minimized SEPHCHC structure was obtained using GAUSSIAN 3.0 revision C.02 (*23*). The polar hydrogen, partial charge, and solvation parameters for use in the AutoDock 3.0.5 simulation were applied using AutoDock Tools. The docking simulations were carried out with the rigid MenH and flexible SEPHCHC. A grid of 60 × 60 × 60 points in the *x*-, *y*-, and *z*-axis directions was built, and the grid center was set to the coordinate of the Nε2 atom of the imidazole ring of His-232. All graphic presentations were generated by PyMol Version 0.99 (*24*).

RESULTS AND DISCUSSION

MenH Sequence Analysis. The MenH proteins have been found to be the most diverse among menaquinone biosynthetic enzymes from different species (*25*). This is consistent with the recent finding that the enzyme has a low energetic burden to stabilize the transition state of the catalyzed reaction (*4*). To better understand the sequence conservation, 47 MenH proteins, including those previously identified in 39 genomes on the basis of a combination of genomic context (the presence of related proteins MenF, MenB, MenD, and MenE in the menaquinone cluster) and homology of the highly conserved MenB protein (*25*) and eight additional sequences identified with the same standards, were withdrawn from GenBank and compared. Except for the putative MenH domain from *Arabidopsis*, all other sequences are from bacteria. Sequence alignments found that MenHs from closely related species show a high level of sequence conservation; for example, MenH from *E. coli* K12 shares 76% amino acid identity with MenH proteins from *Salmonella typhi* Ty2. However, the pairwise identity drops to 49% between *E. coli* MenH and *Yersinia pestis* CO92 MenH, to 29% with MenH of *Bacillus subtilis* subsp. *subtilis str*. 168, and to 27% with MenH from *Nostoc* sp. PCC 7120. As shown in Figure 2, there are only 15 amino acid residues that are strictly conserved in all MenH sequences, including the three amino acid residues in the Ser-His-Asp triad. This low level of sequence conservation demonstrates high divergence in the MenH amino acid sequence.

A MenH phylogenetic tree was obtained from the calculated evolutionary distances between the sequences (Supporting Information). Its branches were consistent with the published prokaryotic phylogenies although the species and protein numbers used in the generation of the MenH phylogenic tree were relatively small. For comparison, phylogenetic trees were also constructed for MenB and MenC (or OSBS/NAAAR family) proteins from the same menaquinone clusters as the MenH proteins. All three trees have a similar topology and resolution in the parts where all the menaquinone enzymes are present, demonstrating that MenH coevolves with other enzymes of the biosynthetic pathway. However, the length of the MenH tree (28.77) is more than four times as big as the MenB tree (6.66) but is marginally smaller than that of the MenC tree (30.71), indicating the high divergence in the MenH proteins. Previous studies have shown that the extremely diverse MenC sequences share fewer than 15 identical amino acid residues with a phylogenetic tree length at least twice as long as that of MenB, MenD, MenE, or other members of enolase superfamily (*26*). Coincidentally, MenC is also an enzyme with a less "burden" to stabilize the transition state (*27*) like MenH (*4*). These results show that both MenH and MenC are indeed much more diverse than other enzymes in the biosynthetic pathway as a result of the low energetic constraint on their evolution.

MenH Active Site and Modeling of the Michaelis Complex. The highly conserved amino acid residues in MenH

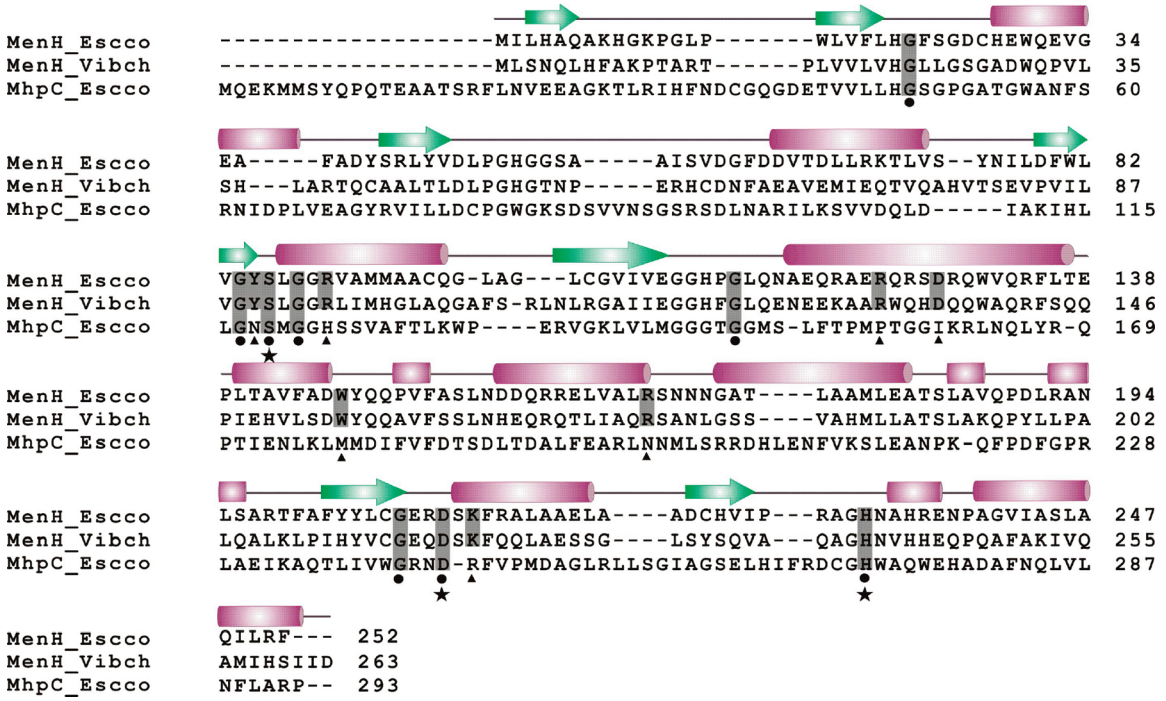

FIGURE 2: Conserved amino acid residues and their locations in the secondary structures of MenH. The alignment of *E. coli* MenH (MenH_Escco), *V. cholerae* MenH (MenH_Vibch), and *E. coli* MhpC (MhpC_Escco) is shown along with the secondary structure of *V. cholerae* MenH (PDB code 1R3D). The shaded amino acid residues are strictly conserved in all 47 MenH sequences from different species in a multiple sequence alignment shown in the Supporting Information. A round dot under the sequences indicates an amino acid residue conserved among MenH proteins which is also found in MhpC, whereas a triangle indicates a conserved MenH residue that is not found in MhpC. Residues in the Ser-His-Asp triad are denoted by a star.

proteins are expected to play important roles either in maintenance of the structural integrity or in the reaction catalyzed by the enzymes. To understand their potential roles, they were mapped on the three-dimensional structure of *E. coli* MenH, which was modeled from the crystal structure of *V. cholerae* protein (PDB code 1R3D). Five glycine residues (Gly-22, Gly-84, Gly-88, Gly-114, and Gly-207) among the 15 strictly conserved amino acid residues were found to locate either at the end of important secondary structures (α-helices or β-sheets) or in the connecting loop regions between them. These glycine residues are also conserved in MhpC in a sequence alignment and found to have the same structural locations as the MenH residues in the structure of *E. coli* MhpC (PDB code 1U2E), which significantly overlap with the cholerae MenH with a low degree of sequence homology (40% identity and 55% similarity). In both proteins, these flexible residues seem to facilitate the conformational change from one major secondary structure to the next in the formation of the overall three-dimensional structures. The high degree of conservation of these residues indicates their critical significance for the integrity of the α/β hydrolase fold structure.

Except Asp-46, six other strictly conserved amino acid residues (Tyr-85, Arg-90, Arg-124, Asp-128, Trp-147, and Lys-212) are located within a short distance from the seryl hydroxyl group of the catalytically essential triad composed of Ser-86, Asp-210, and His-232, which are also strictly conserved in all MenHs as well as in the *E. coli* MhpC protein. These residues are found to line the internal surface of a narrow and deep pocket that contains the catalytic triad and extends to the protein surface (Figure 3A). Since mutagenic analysis has shown that the triad is essential in the MenH-catalyzed reaction (*4*), this pocket is apparently the active site of the enzyme. Noticeably, the deepest end of the narrow pocket is a positively charged amino acid residue, Arg-168, which appears to be involved in the binding of the negatively charged substrate like Arg-188 of MhpC (*14*). Located in a region that is poorly conserved among the MenH proteins, this positively charged residue is found in a majority of the sequences in an unmodified multiple sequence alignment. After manual editing of the sequence alignment, this arginine residue is also conserved in all the MenH proteins, suggesting that it may also be an active site residue important for substrate binding or catalysis.

Only six of the strictly conserved non-glycine residues (Tyr-85, Arg-90, Asp-128, Lys-212, Trp-147, and Arg-168) are found to be uniquely conserved among MenH proteins by comparison of the MenH sequences with the *E. coli* MhpC, whereas Asp-46, Ser-86, Asp-210, and His-232 are also found in MhpC in a sequence alignment (Figure 2). Comparison of the active sites of MhpC and the modeled *E. coli* MenH found that, except the Ser-His-Asp triad, they share little structural similarity despite the fact that both proteins possess the same α/β hydrolase fold and overlap extensively in the three-dimensional structure. This structural difference in active site is consistent with the fact that the two enzymes catalyze mechanistically distinct chemical reactions, although they both rely on the same catalytic triad for the catalysis. The six uniquely conserved amino acids in MenH are expected to play important roles in the substrate binding and stabilization of the transition state.

To understand the interaction between the substrate and the enzyme, the energy-minimized SEPHCHC structure was docked into the MenH structure with AutoDock 3.0.5 (*22*). One hundred distinct structures were obtained in seven clusters using a root mean squared distance (rmsd) tolerance of 1.0 Å with the docking energy ranging from -7.65 to -8.53 kcal·mol^{-1}. A total of 92 structures in six clusters contain the substrate with a slightly different distance from the catalytic triad in the binding pocket that consists of the well-conserved residues as shown in Figure 3A. Only eight structures in one

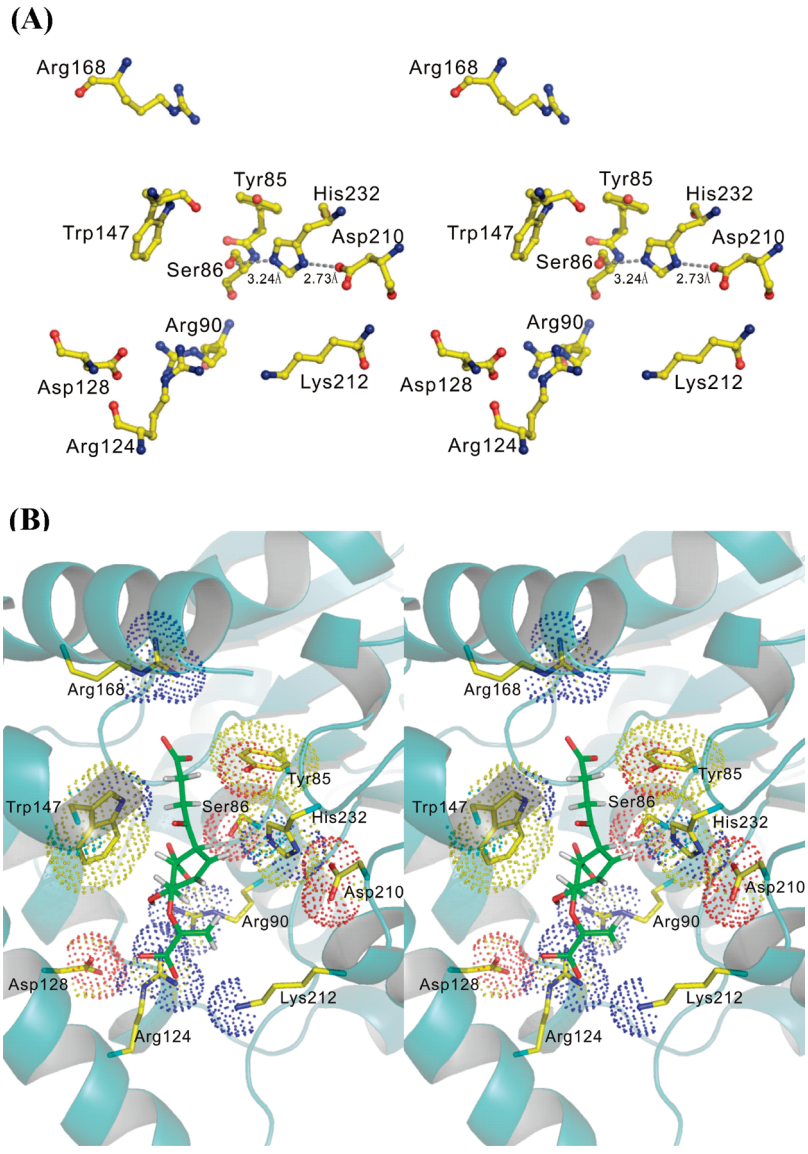

FIGURE 3: (A) Stereoview of the conserved non-glycine amino acid residues of MenH in the modeled structure of *E. coli* MenH. The *V. cholerae* MenH X-ray structure (PDB code 1R3D) is used in the modeling of *E. coli* MenH. (B) Stereoview of the ligand-bound active site of the modeled MenH structure. The complex structure is obtained by docking the optimized substrate structure into the modeled *E. coli* MenH structure. The backbone is shown in ribbon. The side chains of the non-glycine conserved residues are shown in "sticks". The dots show the solvent/protein contact surface of selected residues. The carbon skeleton of the substrate, SEPHCHC, is in green.

(minimum energy: -7.93 kcal·mol^{-1}) of the seven clusters have the substrate completely outside the pocket. A total of 34 structures in two of the clusters are very similar with all the negative charges in the substrate in an appropriate position to interact with a positively charged amino acid side chain on the protein, whereas at least one negative charge of the substrate is not stabilized by a positive residue in all other structures. The structure with the lowest energy in these two clusters (-8.09 kcal·mol^{-1}) was therefore chosen as the model MenH−substrate complex (Figure 3B) despite the fact that the structures in two other clusters are slightly more stable with a minimum energy of -8.53 and -8.33 kcal·mol^{-1}, respectively.

Steady-State Kinetics of the Site-Directed Mutants. To understand how the strictly conserved non-glycine active site residues contribute to catalysis of SHCHC synthesis, they were individually replaced by alanine or other amino acids using site-directed mutagenesis. Tyr-85 was mutated to a phenylalanine to observe the effect of the phenolic hydroxyl group on enzyme catalysis. Some of the point mutants are less stable than the wild-type enzyme, forming precipitates in the purification process. This stability problem was overcome by adding 20% (w/v) glycerol in all of the buffers used in the purification and storage steps and by including 1% glycerol and 0.1% BSA in the buffer for activity assays. All of the purified mutants show a far-UV circular dichroism spectrum that overlaps that of wild-type MenH (data not shown), indicating that their conformation is minimally affected by the point mutations.

The site-directed mutants were characterized by steady-state kinetics as shown in Table 2. For the convenience of comparison, kinetic results for the alanine mutants of the catalytic triad (*4*) are also included in the table. D128A and K212A have the smallest impact on the kinetic properties of MenH among the site-directed mutants of the strictly conserved active site residues. The former has a 7.5-fold K_M increase and 28% k_{cat} decrease while the latter has a modest 1-fold K_M increase and 2-fold k_{cat} decrease in comparison to the wild-type enzyme, suggesting that both residues play a much less significant role in the catalytic process. Indeed, the modeled MenH−SEPHCHC complex shows that

Table 2: Steady-State Kinetic Parameters for Wild-Type MenH and Its Mutants at 25 °C

variant	K_M (μM)	k_{cat} (s^{-1})	k_{cat}/K_M ($M^{-1}\cdot s^{-1}$)	relative k_{cat}/K_M
wild type[a]	10.1 ± 0.8	147 ± 9	$(1.4 \pm 0.5) \times 10^7$	1
S86A[a]	28 ± 3	0.29 ± 0.01	$(1.0 \pm 0.1) \times 10^4$	7.1×10^{-4}
D210A[a]	118 ± 22	0.18 ± 0.02	$(1.5 \pm 0.2) \times 10^3$	1.1×10^{-4}
H232A[a]	8.6 ± 0.3	$(5.8 \pm 0.7) \times 10^{-4}$	67 ± 10	4.8×10^{-6}
H232K	532 ± 49	$(2.1 \pm 0.2) \times 10^{-2}$	39.2 ± 4.0	2.8×10^{-6}
Y85F	14.0 ± 1.2	2.58 ± 0.08	$(1.8 \pm 0.1) \times 10^5$	1.3×10^{-2}
R90A	159 ± 20	$(4.7 \pm 0.3) \times 10^{-2}$	295 ± 16	2.1×10^{-5}
R124A	84.0 ± 9.6	0.51 ± 0.02	$(6.1 \pm 0.5) \times 10^3$	4.4×10^{-4}
D128A	85 ± 13	115 ± 6	$(1.4 \pm 0.2) \times 10^6$	0.10
W147A	23.7 ± 1.5	$(5.6 \pm 0.3) \times 10^{-2}$	$(2.4 \pm 0.1) \times 10^3$	1.7×10^{-4}
W147F	74 ± 13	15.4 ± 2.8	$(2.2 \pm 0.5) \times 10^5$	1.6×10^{-2}
R168A	134 ± 31	2.9 ± 0.4	$(1.5 \pm 0.1) \times 10^4$	1.1×10^{-3}
K212A	19.4 ± 2.8	41.5 ± 2.2	$(2.2 \pm 0.2) \times 10^6$	0.16

[a] Data taken from ref *4*.

neither residue directly interacts with the bound substrate. The side-chain carboxylate of Asp-128 forms a hydrogen bond with the guanidinium group of Arg-124 that is in direct contact with the bound substrate, indicating that this residue serves the function to set a correct orientation for the positive charge of the Arg-124 to bind the substrate. Similarly, Lys-212 is located at a distance from the enoylpyruvyl group of the substrate and is also expected to play a minor role in the catalysis due to the small change in kinetic properties when mutated to alanine.

The large K_M increase observed for alanine mutants of Arg-90, Arg-124, or Arg-168 suggests that these three residues are important for substrate binding. Indeed, these three positively charged residues directly interact with the substrate in the modeled Michaelis complex (Figure 3B): the conserved Arg-168 at the deepest end of the binding pocket forms a salt bridge with the terminal carboxylate group of the 2-succinyl group on the substrate; Arg-90 is involved in another ionic interaction with the carboxylate group at position 1 of the substrate; and the guanidinium group of Arg-124 is at a close distance to the pyruvyl carboxylate group at position 5, which is suitable for the formation of a salt bridge. In the meantime, the large k_{cat} decrease of at least 50-fold for the alanine mutants of these arginine residues (Table 2) strongly suggests that these residues are also involved in the enzymatic catalysis.

In the enzyme−substrate complex model (Figure 3B), the phenolic hydroxyl of the Tyr-85 residue and pyrrolyl NH of the Trp-147 residue are close to the carbonyl oxygen in the 2-succinyl group of SEPHCHC and appear suitable to form hydrogen bonds with the carbonyl group. Removal of the tyrosine phenolic hydroxyl results in a 76-fold k_{cat} decrease and very little K_M change for the Y85F mutant, corresponding to stabilization of the transition state by the hydroxyl group through a weak hydrogen bond (2.56 kcal/mol). On the other hand, replacement of Trp-147 with alanine results in a modest 2.3-fold K_M increase but a precipitous 5800-fold k_{cat} decrease, indicating that this strictly conserved residue is extremely important to MenH catalysis. When this tryptophan residue is replaced by phenylalanine with similar hydrophobicity and bulkiness but without the polar NH group in the side chain, the resulting mutant (W147F) shows a 62.5-fold catalytic efficiency decrease that is likely due to the loss of the transition state stabilization by the side-chain NH. These mutational results and the positioning of the two residues relative to the bound SEPHCHC (Figure 3B) strongly support that the phenolic hydroxyl of the Tyr-85 residue and pyrrolyl NH of the Trp-147 residue stabilize the transition state by forming an "oxyanion hole", which is commonly found in members of the serine protease superfamily (*8*, *9*), the α/β fold hydrolase superfamily (*10*, *11*), and the crotonase superfamily (*28*, *29*). Such an oxyanion hole formed exclusively from amino acid side chain polar groups is found only in a few enzymes such as Δ^5-3-ketosteroid isomerase (KSI) (*30*−*32*). In most other enzymes including subtilisin (*33*−*35*), trypsin and chymotrypsin (*36*, *37*), and all known members of the crotonase superfamily (*28*, *38*, *39*), the oxyanion hole contains at least one backbone NH. The modeled MenH−SEPHCHC complex contains no backbone amide NH close enough to the succinyl carbonyl group of the MenH substrate to be involved in stabilization of an oxyanion-like species in the transition state.

pH−Rate Profiles for Wild-Type MenH and Its S86A Mutant. The pH−rate profiles for the wild-type MenH and its S86A mutant were determined over the pH range 4.5−10 as shown in Figure 4. The log(k_{cat}/K_M)−pH plot of wild-type MenH is bell-shaped, consistent with a simple model (*40*) in which the rate constant depends on ionization of the conjugate acid of an essential base and an essential acid in the free enzyme with a pK_a of 5.6 and 9.4, respectively. In contrast, the MenH log(k_{cat})−pH profile defies such a model by exhibiting a linear relationship with a slope smaller than unity over pH 5.0−7.8 and a zero-slope linear relationship over pH 8.0−10.0. This later plot presents a single inflection point at pH = 8.0, which suggests an essential catalytic base with pK_a = 8.0 for ionization of its conjugate acid in the enzyme−substrate complex. The dramatic difference between the log(k_{cat}/K_M) and log(k_{cat}) profiles is a clear indication that the wild-type enzyme undergoes drastic structural changes when it binds the substrate to form a Michaelis complex. Similarly, a large difference was observed for the two pH−rate profiles of the S86A mutant. The log(k_{cat}/K_M)−pH profile of the mutant is significantly different from that of the wild-type protein and is thus indicative of drastic change in the pH dependence of the enzymatic reaction. However, the log(k_{cat})−pH profile of the mutant has a similar shape as the wild-type enzyme but has its inflection point shifted to pH ≈6.5, suggesting that the mutation significantly changes the basicity of the general base catalyst.

The results from the pH−rate profiling experiments are consistent with a catalytic model in which the side-chain imidazole of His-232 is the essential general base catalyst with a variable pK_a for ionization of its conjugate acid in the reactions catalyzed by both wild-type MenH and its S86A mutant. This proposal is supported by the close distance between the imidazole Nε2 and the abstracted proton of the substrate in the modeled MenH−SEPHCHC complex (Figure 3B). In addition, it is consistent with the fact that the pK_a of the conjugate acid of histidine is sensitive to its environment. In the Ser-His-Asp triad of serine proteases, the histidine side chain has a high basicity due to the special microenvironment (*41*). For example, the active site His-64 of subtilisin has a high pK_a (7.9 ± 0.3 (*42*)) that is close to the pK_a = 8.0 for the general base catalyst as suggested by the log (k_{cat})−pH profile of wild-type MenH (Figure 4B). For histidine residues in other structural contexts, the pK_a of the imidazole side chain varies widely. A great number of such residues, such as His-7, His-37, His-40, and His-48 in the human urokinase kringle domain (*43*) and His-8 of staphylococcal nuclease (*44*), have a pK_a value in the narrow range of 6.2−6.8. Due to this high sensitivity of histidine side-chain acidity to the environment, it is

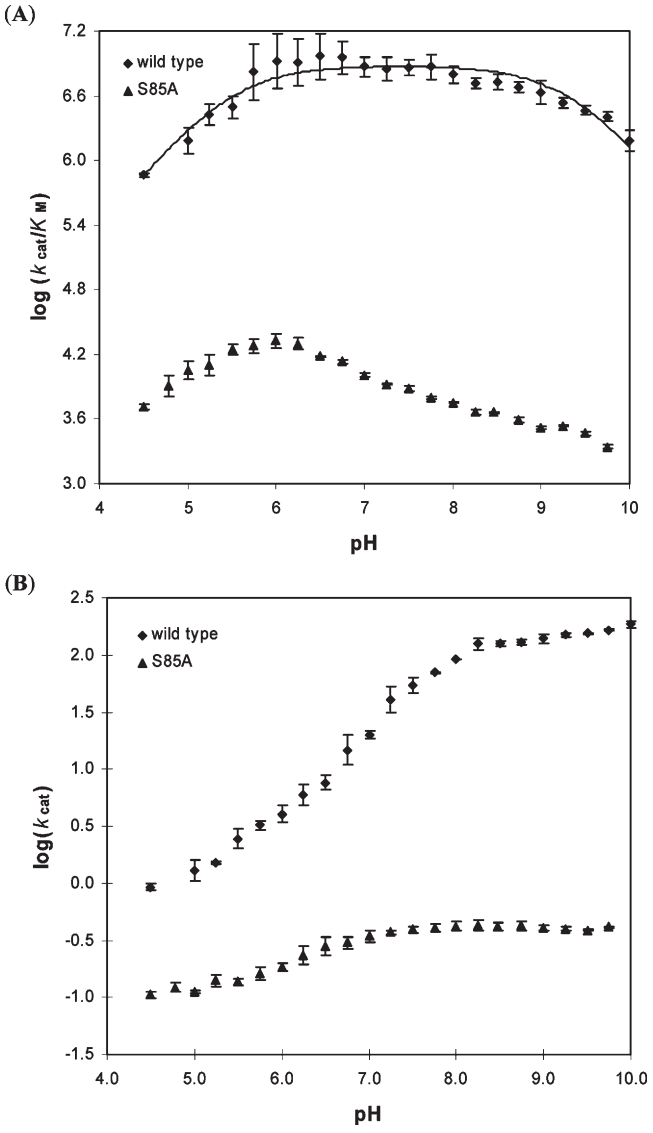

FIGURE 4: pH−rate profiles of the wild-type MenH and its S86A mutant at 22.5 °C. (A) log(k_{cat}/K_M) vs pH. (B) log k_{cat} vs pH. Each data point is the average of three independent measurements. The solid line in (A) is the fitting curve obtained from the equation log Y = log{C/(1 + [H^+]/K_a + K_b/[H^+])}, where Y is k_{cat}/K_M.

very likely that His-232 changes its acidity from pK_a = 8.0 for its conjugate acid as a part of the catalytic triad in the wild-type protein to pK_a = 6.5 in the S86A mutant as indicated by the log (k_{cat})−pH profiles (Figure 4B) in the capacity of an essential general base catalyst. This change may be caused by elimination of a hydrogen bond to the Nε2 of His-232 in the catalytic triad and alteration in solvation of the histidine side chain as well as other residues at the active site by the S86A mutation.

Proton Inventories of MenH and Its S86A Mutant. The proton inventory technique has been widely used to determine the exchangeable proton sites in an enzyme or its substrates that generate a kinetic solvent isotope effect by being involved in the rate-limiting step of an enzymatic reaction (*18*, *45*). In order to obtain further mechanistic information on the proton abstraction reaction catalyzed by MenH, we performed proton inventory experiments by measuring the velocity (v_n) of the SHCHC formation catalyzed by both the wild-type protein and its S86A mutant in different mole fractions of D_2O (n). To avoid a pH effect on the reaction rate, these experiments were carried out in buffers with a pL of 8.75−8.85 on the basis of the pH−rate

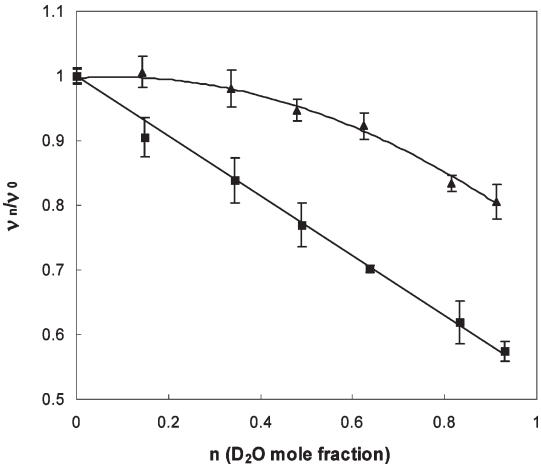

FIGURE 5: Proton inventory curves for the reactions catalyzed by wild-type MenH (■) and its S86A mutant (▲). v_0 is the velocity in 100% H_2O, and v_n is the velocity measured in different mole fractions of D_2O (n). The curve for the wild-type enzyme is fitted to the model that contains a single Φ site in the transition state using the equation $v_n = v_0(1 - n + n\Phi_T)$, where the fraction factor Φ_T = 0.538 (k_H/k_D = 1.86). The curve for the S86A mutant is fitted to the model in which the isotope effect is contributed by a single Φ site in the transition state and a medium effect using the formula $v_n = v_0(1 - n + n\Phi_T)Z^n$, where Φ_T = 0.42 (k_H/k_D = 2.38) and Z = 1.79 (k_D/k_H = 1.79). GraphPad Prism4 is used for the curve fitting.

profiles (Figure 4B). As shown in Figure 5, the proton inventory curve for the wild-type protein is linear, whereas that of the mutant is dome-shaped.

The linear curve clearly indicates that only one exchangeable proton with a kinetic isotope effect (k_H/k_D) of 1.86 is involved in the transition state of the reaction catalyzed by wild-type MenH. On the other hand, there are three possible models consistent with the dome-shaped curve of the S86A mutant by curve fitting (*45*). First, the nonlinear curve may be derived from both a normal isotope effect for a proton in the transition state (isotopic fractionation factor Φ_T = 0.18, corresponding to k_H/k_D = 5.56) and an inverse isotope effect for a proton in the ground state (Φ_R = 0.25, corresponding to k_H/k_D = 4.00). This model is not a realistic description of the mutant-catalyzed reaction because both fractionation factors fall in the range for a transition state hydrogen bridge involved in C−H breakage or tunneling but not in the range for normal solvent-exchangeable protons (*45*). Second, the dome-shaped curve may result from two consecutive rate-determining steps with a weight of 0.59 and a normal isotope effect (Φ_a = 0.54, corresponding to k_H/k_D = 1.85) for the first step and a weight of 0.41 and an inverse isotope effect (Φ_b = 1.82, corresponding to k_D/k_H = 1.82) for the second step. This two-step model is also unlikely because the greatly reduced activity of S86A (*4*) brings the mutant-catalyzed reaction closer to the uncatalyzed SEPHCHC decomposition to SHCHC, for which the based-induced α-proton abstraction is the only possible rate-determining step. Third, the proton inventory curve of the S86A mutant might also result from a single transition state proton site giving rise to a normal isotope effect (Φ_T = 0.42, corresponding to k_H/k_D = 2.38) and a medium effect, or the so-called "Z-site effect" (*45*, *46*), in the inverse direction (Z = 1.79, corresponding to k_D/k_H = 1.79). The last model is a much more likely explanation for the dome-shaped curve of the S86A mutant because the mutation can induce change in solvation of the active site residues to cause the hypothesized medium effect. Thus, results from these model analyses support the involvement of a

transition state proton in the rate-determining step of the reactions catalyzed by both wild-type MenH and its S86A mutant, which gives rise to a comparable kinetic isotope effect.

The proton inventories of MenH and its S86A mutant are similar to those of serine proteases such as trypsin (*47*), chymotrypsin (*47*−*49*), and elastase (*47*, *49*−*51*), which use the same Ser-His-Asp triad for catalysis. In most reactions catalyzed by the serine proteases, the deacylation reaction is the rate-determining step, and it has been found to follow one-proton catalysis for simple substrates with a kinetic isotope effect in the range of 1.4−2.9, like the MenH-catalyzed reaction. In a few cases where the acylation step is rate-determining (*47*, *49*), the proton inventory curve is also linear with one transition state proton contributing to the kinetic isotope effect of a comparable size. This similarity in proton inventory suggests that a similar proton site in the transition state produces the comparable normal kinetic isotope effect in the catalysis of the serine proteases and MenH. For serine proteases, the one-proton catalysis was thought to originate in the general acid−base catalysis by the imidazole of the triad histidine both in acylation and in deacylation (*45*), which is supported by model studies on imidazole-catalyzed hydrolysis reactions (*52*). The so-called proton relay in the triads and the hydrogen bonds stabilizing the oxyanion intermediates were not considered to be a contributor of the detected kinetic isotope effect (*45*, *47*−*51*). By analogy, we propose for MenH and its S86A mutant that abstraction of a proton by the triad histidine-232, the general base catalyst suggested by the pH−rate profiling, either from the triad serine (wild-type MenH) or from an active site water molecule (S86A mutant) is the source of the solvent kinetic isotope effect detected in the proton inventory experiments. Thus, results from the proton inventory experiments support a MenH catalytic mechanism in which the triad histidine acts as a general base to deprotonate the triad serine, leading to formation of a seryl oxide that in turn abstracts an α-proton from SEPHCHC to initiate the 2,5-elimination of pyruvate in the SHCHC synthesis.

No Esterase Activity for MenH. Wild-type MenH has been demonstrated to lack esterase activity toward palmitoyl-CoA and 2,4-dihydroxynaphthoyl-CoA (*4*). The enzyme was tested against additional ester substrates including *p*-nitrophenyl phosphate (*p*NPP), succinyl-CoA, benzoyl-CoA, acetyl-CoA, and 3,5-dihydroxybenzyl-CoA (3,5-DHB-CoA) in order to further characterize its potential esterase activity. No hydrolysis was detected for MenH, while a positive control esterase, EntH or p15 (*4*, *53*), showed high activity toward all ester substrates except acetyl-CoA and *p*NPP (Table 3). These tests provide further evidence that MenH is devoid of hydrolytic activities.

Catalytic Mechanism of MenH. The 2,5-elimination of pyruvate from SEPHCHC by MenH can occur by simultaneous proton abstraction and pyruvate dissociation in a concerted E2 elimination or through a dienolate intermediate in a two-step E1cb mechanism. The one-step elimination is not favored in view of the well-established notion that base-induced *β*-eliminations involving breakage of a C−H bond at an α-position to a carbonyl group proceed by an E1cb mechanism rather than a concerted mechanism (*54*). The two-step mechanism has been shown both by experiments and by theoretical computations to dominate the base-induced 1,4-elimination of allylic ethers (*55*), which is the same type of elimination in the SHCHC synthesis from SEPHCHC. Moreover, a theoretical study found that the base-induced 1,4-elimination of 3-halocyclohexene with a close structural resemblance to the MenH substrate proceeds through a concerted E2 mechanism when the leaving group is chloride but proceeds through an E1cb-like mechanism when the leaving group is fluoride (*56*). In comparison to 3-flourocyclohexene, SEPHCHC has a much more acidic proton in the elimination due to the 2-succinyl group and a poorer leaving group (pyruvyl enolate) than fluoride, both of which strongly favor an E1cb mechanism (*54*−*56*). As such, a stepwise mechanism is favored in the MenH-catalyzed 2,5-elimination of pyruvate from SEPHCHC. In fact, there are ample precedents of E1cb mechanisms in enzymatic reactions in which an electron-withdrawing functionality such as a carbonyl or carboxyl group serves to stabilize the anionic intermediate (*57*−*60*).

Table 3: Hydrolytic Rates of MenH and Control Proteins toward Various Substrates[a]

substrate	EntH (μM/min)	MenH (μM/min)	BSA (μM/min)
palmitoyl-CoA (50 μM)	1.12 ± 0.03	0.013 ± 0.006	0.008 ± 0.003
succinyl-CoA (30 μM)	12.2 ± 0.2	0.03 ± 0.04	0.01 ± 0.01
benzoyl-CoA (100 μM)	46.7 ± 0.1	0.01 ± 0.01	0.00 ± 0.07
3,5-DHB-CoA (50 μM)	37.4 ± 1.8	0.02 ± 0.02	−0.02 ± 0.02
acetyl-CoA (100 μM)	−0.01 ± 0.02	−0.001 ± 0.003	0.01 ± 0.02
pNPP (100 μM)	0.00 ± 0.01	0.02 ± 0.02	−0.01 ± 0.01

[a] The reactions were carried out in 50 mM sodium phosphate buffer (pH 8.0) at room temperature. The concentrations for EntH, MenH, and BSA were all 0.3 μg/mL.

Another issue in MenH catalysis is whether the MenH catalytic triad undergoes a splitting similar to the MhpC triad. In the MhpC-catalyzed reaction, the triad splitting leads to a similar pH−rate profile for both the wild-type protein and its serine-to-alanine mutant because the same Asp-His dyad is the proton-abstracting base in both cases (*13*). However, the pH−rate profiles of wild-type MenH and its S86A mutant are different, suggesting that the MenH catalytic triad is unlikely split in the catalysis like the MhpC triad. Taking this into consideration, a MenH catalytic mechanism is proposed as shown in Figure 6 based on the results from the site-directed mutagenesis, pH−rate profiling, and proton inventory experiments. As discussed above, the triad His-232 is the general base catalyst that serves to deprotonate the serine hydroxyl group of the wild-type enzyme or a water molecule in the S86A mutant to accomplish the α-proton abstraction in the initiation of the elimination reaction.

In the proposed mechanism, the MenH triad plays a very simple role in which the Asp-His dyad serves as a base to deprotonate the serine hydroxyl group in the catalysis. In comparison, the catalytic triad in serine proteases and α/*β* fold hydrolases plays far more complex roles (*8*−*11*). However, the multiple catalytic functions of the triads in serine proteases and α/*β* fold hydrolases are merely an ordered repeat of the simple function of the MenH triad in varied forms. In the MhpC-catalyzed reaction, the Asp-His dyad of the split triad serves as a base to deprotonate the enol proton in the substrate to catalyze keto−enol tautomerization in the first half-reaction and to deprotonate an active site water molecule to generate a hydroxide nucleophile for addition to the carbonyl leading to C−C bond cleavage in the second half-reaction (*13*, *16*). Similarly, in the reactions catalyzed by serine proteases and other α/*β* fold hydrolases (*8*−*11*), the Asp-His moiety of the catalytic triad serves as a base to deprotonate the serine hydroxyl group, exactly like that in the MenH triad, to generate an oxyanion for nucleophilic addition to the scissile carbonyl group in the first

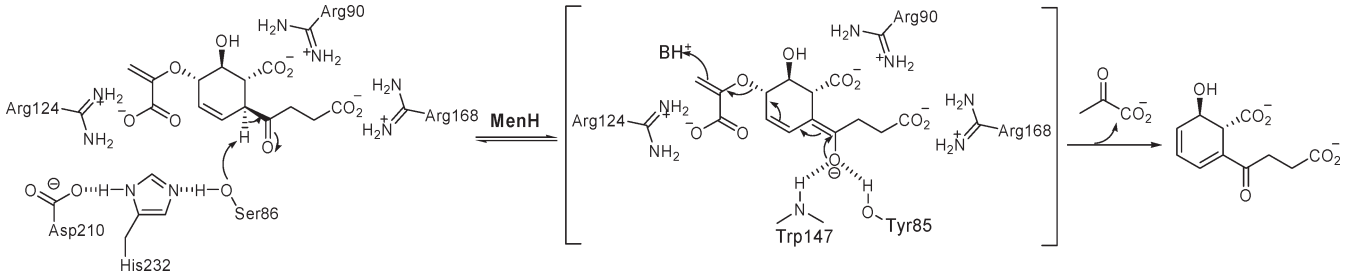

FIGURE 6: Proposed reaction mechanism for the SHCHC synthesis catalyzed by MenH.

half-acylation reaction and again serves as a base to deprotonate an active site water, like the S86A mutant of MenH, to generate a hydroxide for nucleophilic attack in the second half-deacylation reaction. In all reactions catalyzed by serine proteases and α/β fold hydrolases, the conjugate acid formed in the catalytic deprotonation by the Asp-His dyad is integrated into the catalytic process as a general acid, whereas the dyad conjugate acid formed in the MenH-catalyzed reaction is not utilized but is merely deprotonated by the solvent to return to its catalytic form. Therefore, the Ser-His-Asp motif of MenH appears to be an early form of the triad with the simplest but most fundamental catalytic function, from which the sophisticated catalytic roles may be evolved for the triads in serine proteases and α/β fold hydrolases. In connection to this probability, it is interesting to note that MenH may be an ancient enzyme with its catalytic triad formed before those of other triad-utilizing enzymes, because it is one of the biosynthetic enzymes of menaquinone (*1*, *2*), an indispensable respiratory electron transporter in oxygen-poor environments from which all life forms arise.

It is well-known that serine proteases and α/β fold hydrolases are generally active toward a broad range of substrates (*8*−*11*), indicating that the operation of their catalytic triads is little affected by substrate binding. For MhpC that normally catalyzes a C−C bond cleavage reaction, its catalytic triad is also able to generate nucleophile to exhibit esterase activity toward coenzyme A thioesters completely distinct from its cognate substrate (*13*). However, MenH is devoid of any detectable hydrolytic activities, suggesting that its catalytic triad is not operative to generate the reactive seryl oxide in the absence of the cognate substrate SEPHCHC. We propose that the basic seryl oxide is only generated in the MenH triad when the substrate is bound in a conformation suitable for proton abstraction. In other words, the generation of the catalytic base through the triad is coupled to substrate binding, possibly through a substrate-induced conformational change. This speculated conformational change is supported by the dramatic difference between the $\log(k_{cat}/K_M)$ and $\log k_{cat}$ profiles (Figure 4), which represent the pH dependence of the free enzyme and the enzyme−substrate complex, respectively. In addition, it also provides an explanation for the steady-state kinetic properties of the active site mutants R90A, R124A, and R168A, although the kinetic changes could be caused by mutation-induced misalignment of the substrate or intermediate in the active site. Conceivably, single mutations of these active site residues inevitably cause mismatch between the substrate and the binding pocket, which is expected to impair or disable the proposed coupling of base generation to substrate binding to significantly impact the turnover rate. This expected effect is fully consistent with the experimental observations that mutation of these binding site residues causes not only a significant K_M increase but also a significant k_{cat} decrease of greater than 50-fold despite the obvious involvement of these mutated residues only in the SEPHCHC binding but not in any chemical steps of the catalysis.

CONCLUSIONS

MenH is a unique enzyme that adopts a typical α/β hydrolase fold but catalyzes a reaction atypical of α/β hydrolases. We have identified the active site residues in this enzyme by sequence analysis, structural modeling, and site-directed mutagenesis. Steady-state kinetic characterization of the active site mutants has led to identification of three conserved arginine residues (Arg-90, Arg-124, and Arg-168), which are critical to the binding of the tricarboxylate substrate through direct ionic interactions, and two other conserved residues (Tyr-85 and Trp-147) whose polar side chains likely donate hydrogen bonds to form an oxyanion hole. In addition, pH−rate profiling and proton inventory experiments provide evidence that the histidine residue of the MenH triad likely serves as a general base catalyst to deprotonate the serine hydroxyl group, which in turn abstracts an α-proton from the substrate to initiate the 2,5-elimination of pyruvate. These results all point to a MenH catalytic mechanism in which the serine−histidine−aspartate triad carries out a simple but fundamental proton transfer reaction found in the multistep catalysis by the catalytic triads of serine proteases and α/β fold hydrolases, demonstrating nature's ingenuity in using the same structural motif to catalyze different chemical reactions.

SUPPORTING INFORMATION AVAILABLE

Multiple sequence alignment of MenH proteins and phylogenetic trees for MenB, MenC, MenD, and MenH. This material is available free of charge via the Internet at http://pubs.acs.org.

REFERENCES

1. Meganathan, R. (1996) Biosynthesis of the isoprenoid quinones menaquinone (vitamin K2) and ubiquinone (coenzyme Q), in Escherichia coli and Salmonella: cellular and molecular biology (Neidhardt, F. C., Curtiss, R., III, Ingraham, J. L., Lin, E. C. C., Low, K. B., Magasanik, B., Reznikoff, W. S., Riley, M., Schaechter, M., and Umbarger, H. E., Eds.) 2nd ed., Vol. 1, pp 642−656, American Society for Microbiology, Washington, DC.
2. Meganathan, R. (2001) Biosynthesis of menaquinone (vitamin K2) and ubiquinone (coenzyme Q): A perspective on enzymatic mechanisms. *Vitam. Horm. 61*, 173–218.
3. Jiang, M., Chen, M., Cao, Y., Yang, Y., Sze, K. H., Chen, X., and Guo, Z. (2007) Determination of the stereochemistry of 2-succinyl-5-enolpyruvyl-6-hydroxy-3-cyclohexene-1-carboxylic acid, a key intermediate in menaquinone biosynthesis. *Org. Lett. 9*, 4765–4767.
4. Jiang, M., Chen, X., Guo, Z. F., Cao, Y., Chen, M., and Guo, Z. (2008) Identification and characterization of (1*R*,6*R*)-2-succinyl-6-hydroxy-2,4-cyclohexadiene-1-carboxylate synthase in the menaquinone biosynthesis of *Escherichia coli*. *Biochemistry 47*, 3426–3434.
5. Gerlt, J. A., and Babbitt, P. C. (2001) Divergent evolution of enzymatic function: Mechanistically diverse superfamilies and functionally distinct suprafamilies. *Annu. Rev. Biochem. 70*, 209–246.

6. Gerlt, J. A., Babbitt, P. C., and Rayment, I. (2005) Divergent evolution in the enolase superfamily: the interplay of mechanism and specificity. *Arch. Biochem. Biophys. 433*, 59–70.
7. Palmer, D. R. J., Garrett, J. B., Sharma, V., Meganathan, R., Babbitt, P. C., and Gerlt, J. A. (1999) Unexpected divergence of enzyme function and sequence: "*N*-acylamino acid racemase" is *o*-succinylbenzoate synthase. *Biochemistry 38*, 4252–4258.
8. Kraut, J. (1977) Serine proteases: Structure and mechanism of catalysis. *Annu. Rev. Biochem. 46*, 331–358.
9. Warshel, A., Naray-Szabo, G., Sussman, F., and Hwang, J.-K. (1989) How do serine proteases really work?. *Biochemistry 28*, 3629–3637.
10. Ollis, D. L., Cheah, E., Cygler, M., Dijkstra, B., Frolow, F., Franken, S. M., Harel, M., Remington, S. J., Silman, I., Schrag, J., Sussman, J. L., Verschueren, K. H. G., and Goldman, A. (1992) The a/β hydrolase fold. *Protein Eng. 3*, 197–211.
11. Holmquist, M. (2000) Alpha/beta-hydrolase fold enzymes: Structure, functions and mechanisms. *Curr. Protein Pept. Sci. 1*, 209–235.
12. Henderson, I. M. J., and Bugg, T. D. H. (1997) Pre-steady-state kinetic analysis of 2-hydroxy-6-keto-nona-2,4-diene-1,9-dioic acid 5,6-hydrolase: Kinetic evidence for enol/keto tautomerization. *Biochemistry 36*, 12252–12258.
13. Li, C., Montgomery, M. G., Mohammed, F., Li, J.-J., Wood, S. P., and Bugg, T. D. H. (2005) Catalytic mechanism of C-C hydrolase MhpC from *Escherichia coli*: Kinetic analysis of His263 and Ser110 site-directed mutants. *J. Mol. Biol. 346*, 241–251.
14. Dunn, G., Montgomery, M. G., Mohammed, F., Coker, A., Cooper, J. B., Robertson, T., Garcia, J.-L., Bugg, T. D. H., and Wood, S. P. (2005) The structure of the C-C bond hydrolase MhpC provides insights into its catalytic mechanism. *J. Mol. Biol. 346*, 253–265.
15. Fleming, S. M., Robertson, T. A., Langley, G. J., and Bugg, T. D. H. (2000) Catalytic mechanism of a C-C hydrolase enzyme: evidence for a *gem*-diol intermediate, not an acyl enzyme. *Biochemistry 39*, 1522–1531.
16. Li, J. J., and Bugg, T. D. H. (2007) Investigation of a general base mechanism for ester hydrolysis in C-C hydrolase enzymes of the alpha/beta-hydrolase superfamily: a novel mechanism for the serine catalytic triad. *Org. Biomol. Chem. 5*, 507–513.
17. Jiang, M., Cao, Y., Guo, Z. F., Chen, M., Chen, X., and Guo, Z. (2007) Menaquinone biosynthesis in *Escherichia coli*: Identification of 2-succinyl-5-enolpyruvyl-6-hydroxy-3-cyclohexene-1-carboxylate (SEPHCHC) as a novel intermediate and re-evaluation of MenD activity. *Biochemistry 46*, 10979–10989.
18. Schowen, K. B., and Schowen, R. L. (1982) Solvent isotope effects on enzyme systems. *Methods Enzymol. 87*, 551–606.
19. Zhou, Y., Guo, X. C., Yi, T., Yoshimoto, T., and Pei, D. (2000) Two continuous spectrophotometric assays for methionine aminopeptidase. *Anal. Biochem. 280*, 159–165.
20. Larkin, M. A., Blackshields, G., Brown, N. P., Chenna, R., McGettigan, P. A., McWilliam, H., Valentin, F., Wallace, I. M., Wilm, A., Lopez, R., Thompson, J. D., Gibson, T. J., and Higgins, D. G. (2007) Clustal W and Clustal X version 2.0. *Bioinformatics 23*, 2947–2978.
21. Arnold, K., Bordoli, L., Kopp, J., and Schwede, T. (2006) The SWISS-MODEL workspace: a web-based environment for protein structure homology modelling. *Bioinformatics 22*, 195–201.
22. Morris, G. M., Goodsell, D. S., Halliday, R. S., Huey, R., Hart, W. E., Belew, R. K., and Olson, A. J. (1998) Automated docking using a Lamarckian genetic algorithm and an empirical binding free energy function. *J. Comput. Chem. 19*, 1639–1662.
23. Frisch, M. J., Trucks, G. W., Schlegel, H. B., Scuseria, G. E., Robb, M. A., Cheeseman, J. R., Montgomery Jr, J. A., Vreven, T., Kudin, K. N., Burant, J. C., Millam, J. M., Iyengar, S. S., Tomasi, J., Barone, V., Mennucci, B., Cossi, M., Scalmani, G., Rega, N., Petersson, G. A., Nakatsuji, H., Hada, M., Ehara, M., Toyota, K., Fukuda, R., Hasegawa, J., Ishida, M., Nakajima, T., Honda, Y., Kitao, O., Nakai, H., Klene, M., Li, X., Knox, J. E., Hratchian, H. P., Cross, J. B., Adamo, C., Jaramillo, J., Gomperts, R., Stratmann, R. E., Yazyev, O., Austin, A. J., Cammi, R., Pomelli, C., Ochterski, J. W., Ayala, P. Y., Morokuma, K., Voth, G. A., Salvador, P., Dannenberg, J. J., Zakrzewski, V. G., Dapprich, S., Daniels, A. D., Strain, M. C., Farkas, O., Malick, D. K., Rabuck, A. D., Raghavachari, K., Foresman, J. B., Ortiz, J. V., Cui, Q., Baboul, A. G., Clifford, S., Cioslowski, J., Stefanov, B. B., Liu, G., Liashenko, A., Piskorz, P., Komaromi, I., Martin, R. L., Fox, D. J., Keith, T., Al-Laham, M. A., Peng, C. Y., Nanayakkara, A., Challacombe, M., Gill, P. M. W., Johnson, B., Chen, W., Wong, M. W., Gonzalez, C., Pople, J. A. (2004) Gaussian 03, Revision C. 02, Gaussian Inc., Wallingford, CT.
24. DeLano, W. L. (2002) The PyMOL Molecular Graphics System, DeLano Scientific, San Carlos, CA.
25. Glasner, M. E., Fayazmanesh, N., Chiang, R. A., Sakai, A., Jacobson, M. P., Gerlt, J. A., and Babbitt, P. C. (2006) Evolution of structure and function in the *o*-succinylbenzoate synthase/*N*-acylamino acid racemase family of the enolase superfamily. *J. Mol. Biol. 360*, 228–250.
26. Palmer, D. R. J., Garrett, J. B., Sharma, V., Meganathan, R., Babbitt, P. C., and Gerlt, J. A. (1999) Unexpected divergence of enzyme function and sequence: "*N*-acylamino acid racemase" is *o*-succinylbenzoate synthase. *Biochemistry 38*, 4252–4258.
27. Taylor, E. A., Palmer, D. R. J., and Gerlt, J. A. (2001) The lesser "burden born" by *o*-succinylbenzoate synthase: An "easy" reaction involving a carboxylate carbon acid. *J. Am. Chem. Soc. 123*, 5824–5825.
28. Holden, H. M., Benning, M. M., Haller, T., and Gerlt, J. A. (2001) The crotonase superfamily: Divergently related enzymes that catalyze different reactions involving acyl coenzyme A thioesters. *Acc. Chem. Res. 34*, 145–157.
29. Xiang, H., Luo, L., Taylor, K. L., and Dunaway-Mariano, D. (1999) Interchange of catalytic activity within the 2-enoyl-coenzyme A hydratase/isomerase superfamily based on a common active site template. *Biochemistry 38*, 7638–7652.
30. Wu, Z. R., Ebrahimian, S., Zawrotny, M. E., Thornburg, L. D., Perez-Alvarado, G. C., Brothers, P., Pollack, R. M., and Summers, M. F. (1997) Solution structure of 3-oxo-Δ^5-steroid isomerase. *Science 276*, 415–418.
31. Kuliopulos, A., Mildvan, A. S., Shortle, D., and Talalay, P. (1989) Kinetic and ultraviolet spectroscopic studies of active-site mutants of Δ^5-3-ketosteroid isomerase. *Biochemistry 28*, 149–159.
32. Cho, H.-S., Ha, N.-C., Choi, G., Kim, H.-J., Lee, D., Oh, K. S., Kim, K. S., Lee, W., Choi, K. Y., and Oh, B.-H. (1999) Crystal structure of Δ^5-3-ketosteroid isomerase from *Pseudomonas testosteroni* in complex with equilenin settles the correct hydrogen bonding scheme for transition state stabilization. *J. Biol. Chem. 274*, 32863–32868.
33. Bryan, P., Pantoliano, M. W., Quill, S. G., Hsiao, H. Y., and Poulos, T. (1986) Site-directed mutagenesis and the role of the oxyanion hole in subtilisin. *Proc. Natl. Acad. Sci. U.S.A. 83*, 3743–3745.
34. Wells, J. A., Cunningham, B. C., Graycar, T. P., and Estell, D. A. (1986) Importance of hydrogen-bond formation in stabilizing the transition state of subtilisin. *Philos. Trans. R. Soc. London, Ser. A 317*, 415–423.
35. Carter, P, and Wells, J. A. (1988) Dissecting the catalytic triad of a serine protease. *Nature 332*, 564–568.
36. Henderson, R. (1970) Structure of crystalline alpha-chymotrypsin. IV. The structure of indoleacryloyl-alpha-chyotrypsin and its relevance to the hydrolytic mechanism of the enzyme. *J. Mol. Biol. 54*, 341–354.
37. Henderson, R., Wright, C. S., Hess, G. P., and Blow, D. M. (1971) Chymotrypsin: what can we learn about catalysis from x-ray diffraction?. *Cold Spring Harbor Symp. Quant. Biol. 36*, 63–69.
38. Truglio, J. J., Theis, K., Feng, Y., Gajda, R., Machutta, C., Tonge, P. J., and Kisker, C. (2003) Crystal structure of *Mycobacterium tuberculosis* MenB, a key enzyme in vitamin K_2 biosynthesis. *J. Biol. Chem. 278*, 42352–42360.
39. Hamed, R. B., Batchelar, E. T., Clifton, I. J., and Schofield, C. J. (2008) Mechanisms and structures of crotonase superfamily enzymes—How nature controls enolate and oxyanion reactivity. *Cell. Mol. Life Sci. 65*, 2507–2527.
40. Tipton, K. F., and Dixon, H. B. (1979) Effects of pH on enzymes. *Methods Enzymol. 63*, 183–234.
41. Moult, J., Sussman, F., and James, M. N. G. (1985) Electron density calculations as an extension of protein structure refinement: *Streptomyces griseus* protease A at 1.5 Å resolution. *J. Mol. Biol. 182*, 555–566.
42. Day, R. M., Thalhauser, C. J., Sudmeier, J. L., Vincent, M. P., Torchilin, E. V., Sanford, D. G., Bachovchin, C. W., and Bachovchin, W. W. (2003) Tautomerism, acid-base equilibria, and H-bonding of the six histidines in subtilisin BPN′ by NMR. *Protein Sci. 12*, 794–810.
43. Bokman, A. M., Jiménez-Barbero, J., and Llinás, M. (1993) ^{1}H NMR characterization of the urokinase kringle module: Structural, but not functional, relatedness to homologous domains. *J. Biol. Chem. 268*, 13858–13866.
44. Alexandrescu, A. T., Mills, D. A., Ulrich, E. L., Chinami, M., and Markley, J. L. (1988) NMR assignments of the four histidines of staphylococcal nuclease in native and denatured states. *Biochemistry 27*, 2158–2165.
45. Venkatasubban, K. S., and Schowen, R. L. (1984) The proton inventory technique. *CRC Crit. Rev. Biochem. 17*, 1–44.
46. Kresge, A. J., More, O., and Powell, M. F. (1987) Solvent isotopes effects, fractionation factors and mechanisms of proton-transfer

reactions, in Isotopes in Organic Chemistry (Buncel, E., and Lee, C. C., Eds.) pp 177−273, Elsevier, Amsterdam.
47. Elrod, J. P, Hogg, J. L., Quinn, D. M., Venkatasubban, K. S., and Schowen, R. L. (1980) Protonic reorganization and substrate structure in catalysis by serine proteases. *J. Am. Chem. Soc. 102*, 3917–3922.
48. Pollock, E., Hogg, J. L., and Schowen, R. L. (1973) One-proton catalysis in the deacetylation of acetyl-α-chymotrypsin. *J. Am. Chem. Soc. 95*, 968–969.
49. Stein, R. L., Elrod, J. P., and Schowen, R. L. (1983) Correlative variations in enzyme-derived and substrate-derived structures of catalytic transition states. Implications for the catalytic strategy of acyl-transfer enzymes. *J. Am. Chem. Soc. 105*, 2446–2452.
50. Hunkapiller, M. W., Forgac, M. D., and Richards, J. H. (1976) Mechanism of action of serine proteases: tetrahedral intermediate and concerted proton transfer. *Biochemistry 15*, 5581–5588.
51. Stein, R. L. (1983) Catalysis by human leukocyte elastase: substrate structural dependence of rate-limiting protolytic catalysis and operation of the charge relay system. *J. Am. Chem. Soc. 105*, 5111–5116.
52. Patterson, J. F., Huskey, W. P., Venkatasubban, K. S., and Hogg, J. L. (1978) One-proton catalysis in the intermolecular imidazole-catalyzed hydrolysis of esters and amides. *J. Org. Chem. 43*, 4935–4938.
53. Leduc, D., Battesti, A., and Bouveret, E. (2007) The hotdog thioesterase EntH (YbdB) plays a role in vivo in optimal enterobactin biosynthesis by interacting with the ArCP domain of EntB. *J. Bacteriol. 189*, 7112–7126.
54. Bordwell, F. G. (1972) How common are base-initiated, concerted 1,2 eliminations. *Acc. Chem. Res. 5*, 374–381.
55. Bickelhaupt, F. M., Buisman, G. J. H., Koning, L. J., Nibbering, N. M. M., and Baerends, E. J. (1995) Gas-phase base-induced 1,4-eliminations: Occurrence of single-, double-, and triple-well E1cb mechanisms. *J. Am. Chem. Soc. 117*, 9889–9899.
56. Gronert, S., and Kass, S. R. (1997) Theoretical studies of eliminations. 6. The regiochemistry and stereochemistry of the gas-phase reactions of 3-halocyclohexenes with fluoride. An *ab initio* study. *J. Org. Chem. 62*, 7991–8000.
57. Creighton, D. J., and Murthy, N. S. R. K. (1990) in The Enzymes (Sigman, D. S., and Boyer, P. D., Eds.) Vol. 19, pp 397−403, Academic Press, San Diego, CA.
58. Montchamp, J.-L., and Frost, J. W. (1997) Cyclohexenyl and cyclohexylidene inhibitors of 3-dehydroquinate synthase: Active site interactions relevant to enzyme mechanism and inhibitor design. *J. Am. Chem. Soc. 119*, 7645–7653.
59. Basarab, G. S., Steffens, J. J., Wawrzak, Z., Schwartz, R. S., Lundqvist, T., and Jordan, D. B. (1999) Catalytic mechanism of scytalone dehydratase: Site-directed mutagenisis, kinetic isotope effects, and alternate substrates. *Biochemistry 38*, 6012–6024.
60. Gopishetty, B., Zhu, J., Rajan, R., Sobczak, A. J., Wnuk, S. F., Bell, C. E., and Pei, D. (2009) Probing the catalytic mechanism of S-ribosylhomocysteinase (LuxS) with catalytic intermediates and substrate analogues. *J. Am. Chem. Soc. 131*, 1243–1250.